# Systematic study of orientational wetting and anchoring at a liquid-crystal–surfactant interface

G. P. Crawford,* R. J. Ondris-Crawford,† and J. W. Doane
*Liquid Crystal Institute, Kent State University, Kent, Ohio 44242-0001*

S. Žumer
*Physics Department, University of Ljubljana, Jadranska 19, 61000 Ljubljana, Slovenia*
(Received 14 July 1995)

The molecular anchoring and orientational wetting properties of a liquid crystal close to the nematic-isotropic transition temperature confined to the 0.2 $\mu$m cylindrical channels of alumina membranes are investigated for various surface preparations. The cavity walls of the confining pores are chemically modified with an aliphatic acid ($C_nH_{2n+1}$-COOH) to establish surface anchoring. Radical changes in deuterium nuclear magnetic resonance ($^2$H-NMR) line shapes in the nematic phase reveal the existence of a discontinuous homeotropic-to-planar anchoring transition that is induced by either changing the length of the surfactant (vary carbon number $n$), the density of the surfactant on the surface (vary concentration), or by varying temperature. The transition to planar anchoring drives the planar-polar nematic director field to a stable uniform axial structure. Above the nematic-isotropic transition temperature, the thickness of the surfactant monolayer is found to strongly influence the degree of the surface-induced orientational ordering. The corresponding order parameter of the liquid-crystal molecules at the surfactant interface increases as $n$ increases, until a maximum ordering surface ($n=17$) is reached; thereafter, the surface order parameter decreases as $n$ increases. An orientational wetting transition from partial to quasicomplete is observed as the length of the aliphatic acid increases. The effect is manifested in the change of the pretransitional temperature dependence of the adsorption parameter from weak to strong but still nondivergent. Further increase in $n$ results in a reentrant phenomenon back to the partial wetting regime. Similar coupling mechanisms and wetting behaviors exhibited by the long chain aliphatic acids and the more rigid benzoic acid surfactants indicate minimal interdigitation of the liquid-crystal molecules into the surfactant aligning layer.

PACS number(s): 64.70.Md, 61.30.Eb, 68.45.Gd, 61.30.Gd

## I. INTRODUCTION

The presence of a solid surface limiting an organized fluid introduces a rich variety of interfacial phenomena [1]. One of the most extensively studied orientationally ordered fluids is the nematic liquid crystal. The translational symmetry and often also the rotational symmetry of the nematic phase is broken when it encounters an interface. The principal driving force behind the basic interest in surface phenomena of liquid crystals is that they represent simple examples of complex fluids that can exhibit many surface transitions associated with surface-induced order or disorder [2–4], molecular anchoring [5], and orientational wetting [6]: discrete and continuous anchoring transitions [6–20], surface layering transitions [21–26], prewetting transitions [1,4], surface melting [27–29], complete-to-partial orientational wetting transitions [30,31], symmetry breaking transitions [32–35], orientational transitions in monolayers [36], and ordering transitions in microconfined cavities [37–55]. The most attractive surface phenomenon to the general statistical mechanics audience is the Berezinski-Kosterlitz-Thouless (BKT) transition characteristic of systems possessing symmetry of a two-dimensional $x$-$y$ model. In addition to the basic importance of surface phenomena of liquid crystals, understanding the ordering and anchoring mechanics at the liquid-crystal–solid interface is crucial in the fabrication of liquid-crystal displays [56,57].

Anchoring of elongated liquid-crystal molecules on solid surfaces is characterized as planar, tilted, or homeotropic, corresponding to the direction of the long molecular axis: parallel, fixed at an angle, or perpendicular to the plane of the interface, respectively [5]. The first two types can be homogeneous or unidirectional. The energy associated with the direction of the orientation of molecules at the liquid-crystal–solid interface from the preferred direction is called anchoring energy. Rapini and Papoular [58] first proposed the anchoring free energy density to be $f_S = W \sin^2\alpha'/2$, where $\alpha'$ is the angle between the actual and preferred anchoring directions. The constant $W$, known as the molecular anchoring strength, is a measure of the ease at which the orientation can deviate away from its preferred anchoring direction [59,60]. In the nonhomeotropic cases, all directions are not equivalent, and therefore the director orientation at the surface is generally described in terms of the polar $\theta'$ and azimuthal $\varphi'$ anchoring angles [42]. In the extension of the Rapini and Papoular form [58], both principal directions are associated with a polar $W_\theta$ and azimuthal $W_\phi$

*Present address: Palo Alto Research Center, Xerox, 3333 Coyote Hill Rd., Palo Alto, CA 94304.
†Present address: Department of Chemical Engineering, Stanford University, Stanford, CA 94305.

 

anchoring strength, which depend on the topology and chemical nature of the substrate and the liquid-crystal material. There have been numerous measurements of $W_\theta$, ranging between $10^{-3}$ and $10^{-7}$ J/m$^2$, and values of $W_\phi$ are reported to be in most cases an order of magnitude weaker.

In a confined system, anchoring transitions cause structural transitions in the bulk liquid crystal. First order anchoring transitions correspond to the nucleation and growth of domains having a new orientation, and second order anchoring transitions correspond to the appearance of fluctuations creating domains with close orientations. The first observation of an anchoring transition was reported by Ryschenkow and Kleman [7] to be a continuous transition between a conical and homeotropic orientation induced by a temperature change. Similar second order anchoring transitions were reported to occur on free surfaces, glass surfaces treated with a surfactant coupling agent, and SiO films evaporated under oblique incidence [8–20]. Porte [16] observed a continuous anchoring transition as the morphology of the surface was systematically varied. Nazarenko and Lavrentovich recently reported a temperature driven anchoring transition that was found to be influenced by ionic impurities in a nematic liquid crystal composed of centrosymmetric molecules [20].

First order anchoring transitions have also been reported to occur between different monostable planar anchoring on gypsum and two-tristable planar anchoring on mica surfaces [17]. Kitzerow has observed similar transitions by physically deforming a mica surface [18]. Recently, Strigazzi and co-workers observed a discontinuous transition from homeotropic-to-planar anchoring on lecithin treated glass surfaces [13].

The study of anchoring ordering mechanisms of liquid crystal confined to a restricted geometry has burgeoned over the past few years because of the importance of confinement in liquid-crystal display technologies [56,57] and the basic interest of finite size effects in both well defined and random confining geometries [37–55]. Much of the basic interest in the ordering in confined liquid-crystal systems was pioneered by Golemme and co-workers [61,62]; they confirmed Sheng's prediction [4] that the nematic-isotropic transition becomes continuous when the confining volume reaches a critical diameter. In the orientationally ordered phase, confined liquid crystals present a very challenging problem because one must account for the elastic constraint associated with the curvature of the cavity as well as the surface anchoring. To complicate the problem even more, surface elastic terms enter into the free energy for nematic director fields that depend on more than one Cartesian coordinate, covering the effects of surface anchoring. Deuterium nuclear magnetic resonance ($^2$H-NMR) has made a significant contribution in determining nematic director fields and important surface parameters in submicrometer cavities where surface effects beocme pronounced. The first simultaneous measurement of the polar and azimuthal molecular anchoring strength and the saddle-splay surface elastic constant has recently been reported using well defined cylindrical cavities (diameters $<1$ $\mu$m). Deuterium NMR was also used to observe a discontinuous anchoring transition from homeotropic-to-planar anchoring conditions in alumina membranes by changing the carbon number of the aliphatic acid surface coupling agent at the cavity wall. Kralj and co-workers have employed the NMR technique to study homeotropic anchoring conditions in random silica matrices [49].

A phenomenon closely related to surface anchoring that occurs above the nematic-isotropic bulk phase transition at confining surfaces is orientational wetting. A quantity used to categorize the wetting regime is the adsorption parameter $\Gamma$, defined as $\Gamma=\int_0^\infty [S(z)-S_B]dz$ in the case of uniaxial ordering, where $S(z)$ and $S_B$ are the orientational order parameters in the surface layer and bulk liquid crystal, respectively, and $z$ is the distance from the surface [6,27,30,31]. As the temperature approaches the nematic-isotropic transition from above, $\Gamma$ will either diverge to infinity (complete wetting) or will remain finite (partial wetting). The wetting regime strongly depends on the nature of the liquid-crystal–solid interaction.

Sluckin and Poniewierski have qualitatively investigated the critical behavior of $\Gamma$ in the case of complete wetting [63]. A power law of the form $\Gamma\sim\Delta t^{-1/3}$ is obtained for van der Waals type interactions, where $\Delta t$ is reduced temperature $(T-T_{\rm NI})/T_{\rm NI}$, $T$ is the actual temperature, and $T_{\rm NI}$ is the nematic-isotropic transition temperature. A much weaker logarithmic divergence is predicted, $\Gamma\sim\ln(\Delta t)$, for interactions that are of the short range type. This logarithmic divergence is consistent with the Landau–de Gennes phenomenological description. A Fréedericksz-type wetting transition gives another power law of the form $\Gamma\sim\Delta t^{-1/2}$.

A number of experiments have confirmed the logarithmic wetting phenomena of liquid crystals at a solid surface [6,27,30,31]. Miyano [6] pioneered the study of surface-induced order and provided the first experimental evidence of surface-induced nematic order. Shen and co-workers expanded on this work using evanescent wave ellipsometry to characterize the wetting regimes of alkyl cyanobiphenyl liquid crystals ($n$CB) [30]. They found that complete wetting is evident for 6CB-9CB, while only partial wetting is realized for 5CB on glass plates coated with silane. A transition from quasicomplete to partial wetting has been confirmed in confined systems using $^2$H-NMR, where the carbon number of the surface coupling molecule at the cavity wall is varied to induce the transition [31]. The term quasicomplete wetting was introduced for the situations in which very pronounced, but nondivergent, pretransitional increases of the adsorption parameter $\Gamma$ were observed as the isotropic-nematic transition was approached.

The phenomenological surface free energy density used to describe pretransitional order and disorder is developed from the Landau-type expansion in terms of the order parameter. Sheng [4] first used a surface free energy density linear in the scalar order parameter $S$ of the form $f_S=-GS\delta(z)$, where $G$ is the surface coupling constant. This form predicts surface-induced order and a spontaneous surface boundary layer transition for certain

magnitudes of $G$. Sluckin and Poniewierski [32] have used a quadratic form of the surface free energy density $f_S=(-GS+US^2/2)\delta(z)$, where $G$ and $U$ correspond to ordering and disordering surface coupling constants, respectively. To also cover the nonuniaxial cases, where order is described by tensor order parameter Q, Nobili and Durand [64] have implemented a similar but more intuitive quadratic form $f_S=g(\mathrm{Q}-\mathrm{Q}_S)^2\delta(z)$, where $g$ is the surface coupling constant and $\mathrm{Q}_S$ is the preferred surface form of the tensor order parameter. The latter two forms of the surface free energy density are quadratic in $S$ with two adjustable parameters. The quadratic coupling in the planar anchoring case yields a variety of surface phenomena, and in particular allows for the possibility of disorder and symmetry (BKT-type) breaking surface transitions [32–35].

There is growing theoretical interest in the literature on pretransitional nematic surface ordering corresponding to a negative orientational order parameter [31–35]. A negative orientational order parameter can arise when the liquid-crystal molecules favor random planar alignment. It is predicted that random planar alignment on approaching the nematic-isotropic transition temperature becomes unstable with respect to a biaxial phase. This transition is continuous and therefore of the BKT type. Moses and Shen [29] have used evanescent wave ellipsometry to show the existence of a negative surface orientational order parameter, measured to be $-0.047$, at the surface above the nematic-isotropic transition. Deuterium NMR measurements are also showing weak negative surface order parameters of $-0.030$ for short chain surfactant molecules attached to the cavity walls of alumina membranes [31]. To our knowledge, there have been no reported observations of the BKT symmetry breaking transition to date.

Although there is a relatively large amount of experimental data on surface anchoring and pretransitional ordering, the details about the interactions occurring at the surface are not completely understood. We attempt to gain as much physical insight as possible by presenting a comprehensive study of molecular anchoring, orientational wetting, and ordering close to the nematic-isotropic transition. We have designed experiments to systematically control the liquid-crystal–solid interaction using different surfactant molecules to treat the cylindrical channels of alumina membranes. A deuterated liquid-crystal material is filled in these cavities and probed with $^2$H-NMR. We demonstrate the systematic behavior of anchoring and wetting in terms of the length and type of the surfactant coupling agent and density of surfactant molecules on the surface. Our results are analyzed in terms of two well known phenomenological approaches: Frank elastic theory in the nematic phase and the Landau–de Gennes approach in the isotropic phase.

This contribution is organized in the following manner. Section II is devoted to the confining materials and the surface treatment process. Section III describes the application of NMR to confined liquid-crystal systems. Section IV is the application of elastic theory to cylindrical systems and the presentation of the $^2$H-NMR line shapes in the nematic phase showing the existence of a discrete structural transition. Section V is devoted to pretransitional ordering and disordering as well as orientational wetting properties. The characterization of the wetting regime and the magnitude and sign of the surface order parameter for a wide variety of surfactant covered surfaces are presented. We conclude in Sec. VI.

## II. MATERIALS

The cylindrical channels of Anopore membranes [65–67] with chemically modified cavity walls proved to be a convenient system to study microconfined liquid crystals [31,38,68]. Here the pores were permeated with the liquid-crystal compound 4′-pentyl-4-cyanobiphenyl (5CB-$\alpha d_2$) deuterated in the $\alpha$ position of the hydrocarbon chain. The membranes are composed of a high purity alumina matrix with 0.2 $\mu$m diam cylindrical channels that penetrate through its 60 $\mu$m thickness [Fig. 1(a)]. The porosity of Anopore membranes has been measured to be 40%, making them ideal systems to study confinement and finite size effects of materials with integrative techniques.

The cavity walls of the channels were chemically treated with different surfactants prior to the introduction of liquid crystal. Surfactants employed in this study [Fig. 1(b)] are aliphatic acids and a benzoic acid. A 2–4 % by weight solution of the surfactant in methanol was prepared. The membranes were soaked in the solution for 1 min to ensure complete filling of the channels. The membrane was removed from the solution, sandwiched

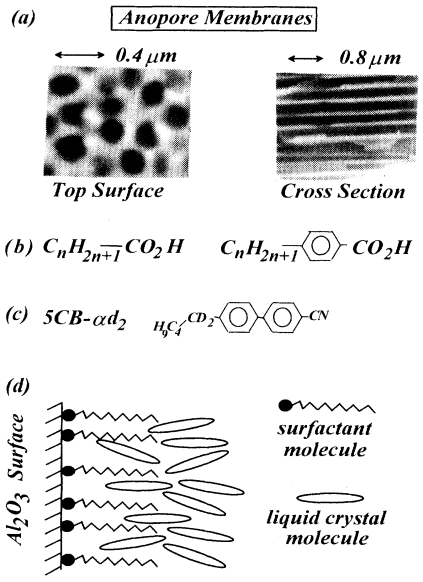


FIG. 1. Scanning electron microscope photograph of Anopore membranes (a) showing the cylindrical nature of the confining pores. (b) The aliphatic and benzoic acid surfactants used to treat the inner cavity wall of the $Al_2O_3$ Anopore membranes. (c) The deuterated low molecular weight liquid-crystal 5CB deuterated in the $\alpha$ position on the hydrocarbon chain. (d) A simple model to demonstrate the interaction between the aliphatic acid surface treatment and the liquid-crystal molecules.

between two Whatmann filtration papers to remove excess solution from the surface, and placed under vacuum for 1 h at 140 °C. The membranes were then cut into $5\times25$ mm$^2$ strips and filled with 5 CB-$\alpha d_2$ [Fig. 1(c)]. Approximately 40 strips were stacked on one another and sealed in a 5 mm diam thin walled NMR tube. This provided a sufficient signal-to-noise ratio for a $^2$H-NMR experiment.

A schematic illustration of the phenomena occurring at the surface is presented in Fig. 1. If the aliphatic chains of an aliphatic acid form a compact assemblage perpendicular to the cavity wall, the liquid-crystal molecules may also orient perpendicular to the cavity wall if the aliphatic chain is of sufficient length [31].

## III. DEUTERIUM NUCLEAR MAGNETIC RESONANCE ($^2$H-NMR)

### A. Nematic phase

The most desirable way to observe nematic director fields is with optical polarizing microscopy; however, this is impossible with cavity diameters well below the optical resolution limit. Deuterium NMR is ideal for such a study since it is sensitive to the nematic director distribution via the quadrupole splitting frequency [69]

$$\delta\nu=\tfrac{1}{2}S(r)\delta\nu_0\{[3\cos^2\theta(\mathbf{r})-1] +\eta(\mathbf{r})\sin^2\theta(\mathbf{r})\cos2\psi(\mathbf{r})\}\ , \tag{1}$$

where $\theta(\mathbf{r})$ and $\psi(\mathbf{r})$ express the orientation of the **B** field in the frame of the local electric field gradient (EFG) tensor averaged over fast orientational fluctuations, and $\delta\nu_0$ is the bulk quadrupole splitting in the perfectly ordered phase. The asymmetry parameter $\eta(\mathbf{r})$ is zero for uniaxial liquid crystal, but it can become nonzero if the averaging motions (orientational fluctuations) lose their symmetry under confinement. This effect is predicted to be small and is neglected in our studies [$\eta(\mathbf{r})=0$] [32]. Only two absorption peaks are expected for an aligned bulk nematic phase selectively deuterated at a specific site on the molecule.

The analysis of nematic structures in our 0.2 $\mu$m channels is simplified by the absence of motional averaging [70]. Using the diffusion relation $x_0\sim(D/\delta\nu_B)^{1/2}$, where $D$ is the diffusion constant and $x_0$ is the distance the molecule migrates during the characteristic time $\delta\nu_B^{-1}$, the molecule migrates $x_0\sim0.02$ $\mu$m for values of $D=10^{-11}$ m$^2$/s and $\delta\nu_B=50$ kHz. The spectra therefore reflect a static director distribution since $x_0$ is much less than cavity diameters. To pinpoint the director field within the cavities more accurately from the $^2$H-NMR spectrum, two orientations of the cylindrical axis in the magnetic field are studied: $\theta_B=0°$ corresponds to the cylindrical axis being parallel to the **B** field, and $\theta_B=90°$ corresponds to the cylindrical axis being perpendicular to the **B** field.

### B. Deuterium NMR in the isotropic phase

The $^2$H-NMR spectra in the isotropic phase are analyzed differently than in the nematic phase because complete motional averaging over the cylinder is realized. The molecule migrates a distance $x_0\sim(D/\delta\nu)^{1/2}$ during the NMR measurement, which is $>100$ nm for $D=10^{-11}$ m$^2$/s and $\delta\nu<1$ kHz [31,38,39]. The resulting quadrupole splitting given by Eq. (3), neglecting biaxiality, is averaged over the cylindrical cross section to incorporate the inhomogeneity in the orientational order parameter

$$\langle\delta\nu\rangle=\langle S(\mathbf{r})\rangle\delta\nu_0[\tfrac{3}{2}\langle\cos^2\theta(\mathbf{r})\rangle-\tfrac{1}{2}]\ , \tag{2}$$

where $\langle\cos^2\theta(\mathbf{r})\rangle$ and $\langle S(\mathbf{r})\rangle$ are averaged separately since they are uncorrelated.

The power of the $^2$H-NMR technique is evident in the isotropic phase of our systems since the averaged splitting $\langle\delta\nu\rangle$ is a direct measure of the adsorption parameter given by the following integrand:

$$\Gamma=\int_0^\infty S(z)dz\approx\frac{1}{2\pi R}\int_0^\infty S(z)2\pi r\,dr=\frac{R}{\kappa}\langle\delta\nu\rangle/\delta\nu_0\ , \tag{3}$$

which characterizes the effective thickness of the ordered layer. We recognize that the correlation length of nematic order $\xi$ is much less than the radius $R$ ($\xi\ll R$) in our situation. The parameter $\kappa$ is a geometrical factor arising from the direction of the nematic director with respect to the magnetic field direction; it is 1 for perpendicular anchoring in the cavity and 2 for parallel anchoring in the cavity. Monitoring $\langle\delta\nu\rangle$ as a function of temperature as the nematic-isotropic phase transition is approached from above reveals if the orientational wetting at the cavity wall is complete ($\Gamma$ diverges) or partial ($\Gamma$ remains finite). The temperature dependence of $\Gamma$ (or $\langle\delta\nu\rangle$) can be understood on the basis of the Landau–de Gennes (LdG) model, which is developed in Sec. V to yield $\Gamma_{\mathrm{LdG}}$.

Although $^2$H-NMR is an integrative technique, it is also sensitive to the contribution of a single molecular layer as described in our previous work [31,38,39]; particularly important is the first molecular layer. Its effective thickness $l_0$ is estimated by averaging over the squares of the molecular length $q$ and the molecular diameter $d$ to yield

$$l_0=[(q^2+2d^2)/3+2S_0(q^2-d^2)/3]^{1/2}\ . \tag{4}$$

In the weakly ordered phase with surface value of the order parameter $S_0\ll1$, the thickness $l_0$ is estimated to be $\sim1.2$ nm using values of $q=2.0$ nm and $d=0.5$ nm. The behavior of the order parameter within this layer cannot be described with a continuum model. This must be taken into account when experimentally determining the value of the order parameter at the surface $S_0$ from $\langle\delta\nu\rangle$ by comparing $\Gamma$ in Eq. (3) to the theory. We assume that $S_0$ is constant in an effective first molecular layer of thickness $l$, and then it follows the continuum theory. This will be described in more detail in Sec. V and can be realized by supplementing the Landau–de Gennes adsorption parameter $\Gamma_{\mathrm{LdG}}$ with an effective first layer correction $lS_0$. Although a simple guess leads $l=\frac{1}{2}l_0$, we will use $l=l_0$, as was deduced from the best fits between experiment and theory in our previous work [31,38,39].

## IV. NEMATIC PHASE

### A. Elastic theory

In general, confinement breaks the symmetry of the nematic phase, and the resulting structure of the nematic director-field depends on elastic forces, surface coupling, and external fields. The total free energy of a confined liquid crystal is within the Frank elastic approach and therefore expressed as [42]

$$F=\frac{1}{2}\int_{\text{vol}}\{K_{11}(\nabla\cdot\mathbf{n})^2+K_{22}(\mathbf{n}\cdot\nabla\times\mathbf{n})^2+K_{33}(\mathbf{n}\times\nabla\times\mathbf{n})^2-K_{24}\nabla\cdot(\mathbf{n}\times\nabla\times\mathbf{n}+\mathbf{n}\nabla\cdot\mathbf{n})\}dV-\frac{1}{2}\frac{\Delta\chi}{\mu_0}\int_{\text{vol}}(\mathbf{B}\cdot\mathbf{n})^2dV$$
$$+\frac{1}{2}\int_{\text{surf}}(W_\phi\sin^2\phi+W_\theta\cos^2\theta)\sin^2\theta\,dA\ , \tag{5}$$

where $K_{11}$, $K_{22}$, and $K_{33}$ are the traditional splay, twist, and bend bulk elastic constants, respectively, and $\mathbf{n}$ represents the direction of the local nematic director. The saddle-splay surface elastic constant $K_{24}$ is a material parameter that is independent of the interactions occurring at the surface. The fourth term incorporates the effects of the magnetic field $\mathbf{B}$, with $\Delta\chi$ being the anisotropy in diamagnetic susceptibility. The final term represents an anisotropic part of the interfacial free energy described by the azimuthal $W_\varphi$ and polar $W_\theta$ anchoring strengths, as well as the azimuthal $\varphi$ and polar $\theta$ anchoring deviation angles [42]. Before we proceed with the discussion on the stable nematic director fields derived from Eq. (5), it is worthwhile at this point to show that the magnetic field term in Eq. (5) is negigible for the 4.7 T field strength of our NMR spectrometer. The magnetic coherence length is given by $\xi_m=(\mu_0K/\Delta\chi)^{1/2}B$, where $K=7\times10^{-12}$ J/m and $\Delta\chi=2.8\times10^{-7}$ are the average elastic constant and diamagnetic susceptibility, respectively, for the 5CB compound. The calculated value $\xi_m\sim1.7$ $\mu$m is substantially larger than the 0.2 $\mu$m cavity diameters of Anopore membranes; therefore, the magnetic field term in Eq. (5) is neglected.

First we consider the director configurations with homeotropic anchoring described by $W_\phi=W_\theta$. For samples of large radii and sufficiently strong anchoring, a nonplanar arrangement called the escaped-radial configuration appears [Fig. 2(a)], first discussed by Cladis and Kleman [71], Meyer [72], and Saupe [73] and later extended by Allender, Crawford, and Doane [40] and Kralj and Žumer [74] to the weak anchoring regime. A planar-radial structure is also possible when $K_{33}\gg K_{11}$ and strong anchoring at the surface is realized [Fig. 2(b)] [40,70–73]. In small radii with sufficiently weak anchoring conditions, a planar-polar structure is stable [Fig. 2(c)] [40,44,74,75]. The stability diagrams among the planar-polar, escaped-radial, and planar-radial structures have been presented elsewhere [40,44,74,75].

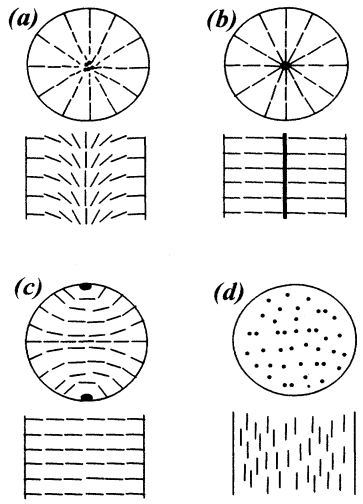


FIG. 2. Four possible nematic director-fields in a cylindrical cavity: (a) the escaped radial, (b) the planar radial, (c) the planar polar, and (d) the parallel axial.

The free energy of the planar-polar structure in its analytical form for $K_{11}=K_{33}=K$ is given by the relation [40]

$$F_{\text{PP}}=\pi K[-\ln(2\xi\gamma)+(1-\gamma)/\xi]\ , \tag{6}$$

where $\gamma=(\xi^2+1)^{1/2}-\xi$, $K=K_{11}=K_{33}$, $\xi=2K/RW_\theta$, and $R$ is the radius of the cavity. As can be seen in Eq. (6), the stability of the planar-polar structure depends on the polar anchoring strength $W_\theta$. For small values of $RW_\theta/K$ (i.e., $\xi\to\infty$), Eq. (6) reduces to $F_{\text{PP}}=\pi RW_\theta/2K$.

There are a wide variety of possible stable nematic director fields when planar anchoring conditions are present at the cavity wall of cylindrical samples [38]. The director fields have been treated in detail for concentric anchoring direction at the cylinder wall [42]. Such structures are possible only when concentric grooves or corrugations are present at the inner cavity wall of the cylinder. If cavity walls are smooth or no topological constraints (grooving or scratching) are introduced ($W_\phi=0$), the director field is usually in a parallel axial arrangement [Fig. 2(d)].

### B. Aliphatic acid surfactant

The spectra for the 2% aliphatic acid surface treatment recorded at room temperature are presented in Figs. 3(a) and 3(b). It is evident from the spectra that an abrupt configurational change has occurred between $n=6$ and 7. For the $n=5$ and 6 surfaces, the $\theta_B=0°$ spectra are identical to the macroscopically aligned bulk nematic phase spectrum with a quadrupole splitting of $\delta\nu_B$, while the $\theta_B=90°$ spectra have a quadrupole splitting of $\frac{1}{2}\delta\nu_B$. These spectra are completely described by

the uniform axial structure with planar anchoring conditions. For the $n=20$, 18, 17, 15, 9, and 7 surfaces, the $\theta_B=0°$ spectra consist of two sharp peaks with a quadrupole splitting frequency of $\frac{1}{2}\delta\nu_B$, indicative of a planar director field orthogonal to the cylindrical axis. At $\theta_B=90°$, a classical cylindrical powder pattern is recorded for $n=20$, 18, 17, 15, 9, and 7. These spectra are consistent with both the planar-polar and planar-radial structures [see Figs. 2(b) and 2(c)] with homeotropic anchoring conditions; however, $K_{33}/K_{11}$ is $\sim 1.4$ for 5CB at room temperature, which excludes the planar-radial structure since it requires $K_{33}/K_{11} \gg 1$ [40,44]. The symmetry axes of the planar-polar director fields are therefore randomly distributed around the **B** field. A free energy estimate confirms that only slight deviations away from the circular cross section of a few percent prevent the **B** field of the NMR spectrometer from orienting the symmetry axis.

The spectra for the 4% aliphatic acid surface treatment recorded at room temperature are presented in Fig. 4 for $n=15$, 6, and 5 surfaces. The spectra show a structural change between the $n=5$ and 6 surfaces. The $n=5$ sample is described by the uniform axial structure, while the $n=6$ and 15 are described by the planar-polar structure. The only difference between the 2% and 4% surface treatments is that the structural change has been shifted down to a smaller $n$ for the higher concentration of surface treatment solution.

The temperature dependence of two samples ($n=7$ for 2% and $n=6$ for 4%) with homeotropic anchoring was studied just below the transition point to see if the structural transition can be induced thermally. We choose these samples to study the temperature dependence because it is the last value of $n$ at which homeotropic anchoring is found stable, before reverting to a planar alignment for smaller $n$. The $\theta_B=0°$ spectra are presented in Fig. 5. The $n=7$ surface for the 2% concentration shows no signs of a structural transition taking place as the nematic-isotropic phase transition is approached; however, the $n=6$ surface for the 4% concentration shows growing of additional peaks that are separated by $\delta\nu_B$ as the nematic-isotropic phase is approached from below. This indicates that the discontinuous nature of the anchoring transition can be induced by a temperature change. The transition to complete planar anchoring did not occur in all cavities because the $\frac{1}{2}\delta\nu_B$ splitting persists very close to the transition. We attribute this to

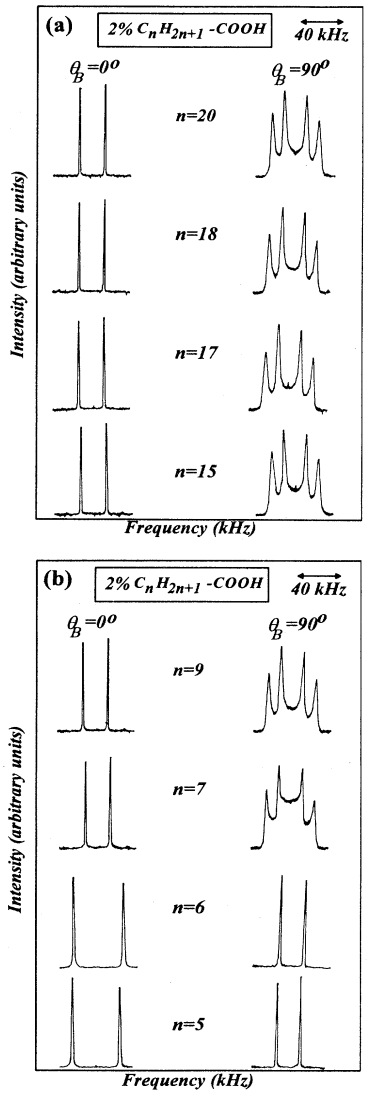


FIG. 3. $^2$H-NMR line shapes of 5CB-$\alpha d_2$ confined to the surfactant treated (2% $C_nH_{2n+1}$-COOH) cavities of Anopore membranes accumulated in the nematic phase $T_{NI}-T=10.5$ K for (a) long and (b) short lengths of the aliphatic chain. The spectra are consistent with the planar-polar structure for $n>7$ and the parallel axial for $n<6$.

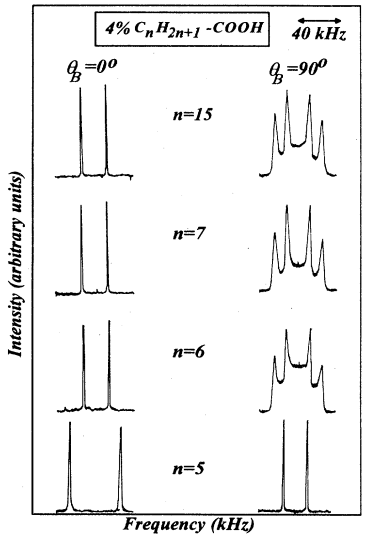


FIG. 4. $^2$H-NMR line shapes of 5CB-$\alpha d_2$ confined to the surfactant treated (4% $C_6H_{2n+1}$-COOH) cavities of Anopore membranes accumulated in the nematic phase at $T_{NI}-T=10.5$ K for various lengths of the aliphatic chain. The spectra are consistent with the planar-radial structure for $n>6$ and the parallel axial for $n<5$.

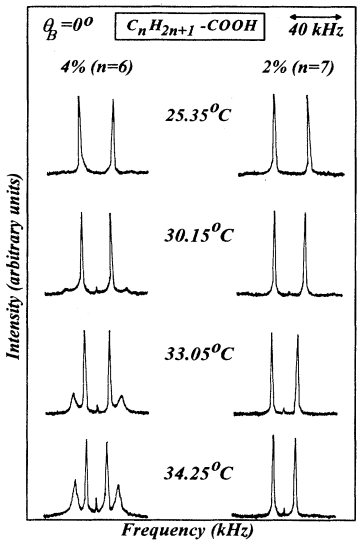


FIG. 5. $^2$H-NMR line shapes of 5CB-$\alpha d_2$ confined to the surfactant treated ($C_nH_{2n+1}$-COOH) cavities of Anopore membranes accumulated in the nematic phase as a function of temperature for the 4% and 2% concentrations. The 4% $n=6$ sample is showing a transition from the planar-polar to the parallel-axial structure as the temperature is increased.

some of the cylinders not reverting to the planar anchoring. This is plausible since the anchoring transition is very sensitive to both the carbon number of the aliphatic chain and concentration of surface treatment solution. We have not observed this temperature driven transition for the 4% $n=7$ surface.

### C. Benzoic acid surfactant

Deuterium NMR spectra for a 2% benzoic acid surface recorded at room temperature are presented in Fig. 6. The $\theta_B=0°$ surface spectrum consists of two sharp peaks separated by $\frac{1}{2}\delta\nu_B$, and the $\theta_B=90°$ is the typical cylindrical powder pattern. This indicates that the structure is planar polar, similar to the $n>6$ samples for the 2% aliphatic acid surface treatment and $n>5$ for the 4% aliphatic acid surface treatment.

### D. Analysis of results in the nematic phase

The strength of the NMR technique lies in determining nematic structures and structural transitions within sub-

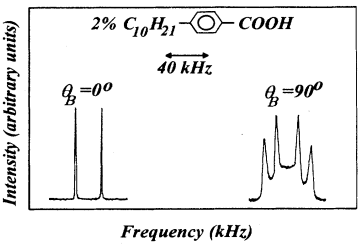


FIG. 6. $^2$H-NMR line shapes of 5CB-$\alpha d_2$ confined to the surfactant treated (benzoic acid) cavities of Anopore membranes accumulated in the nematic phase at $T_{NI}-T=10.5$ K showing the planar-polar structure.

micrometer cavities that are too small to be resolved by an optical microscope. Determining the actual anchoring direction, however, is beyond the capabilities of the NMR technique because it is only sensitive to the director distribution; furthermore, the analysis is complicated by the large elastic constraint introduced by the cylindrical geometries.

The structural transition occurring in the cavities when the carbon number $n$ of the surfactant molecule is varied is driven by a more fundamental phenomenon, an anchoring transition. This transition can be described by two models: (1) $W_\theta$ decreases as $n$ decreases in supporting homeotropic anchoring until $W_\theta$ changes sign, or (2) there is a continual change of the preferred anchoring angle $\theta_0$ (measured from the surface normal) from $\theta_0=0$ to $\pi/2$. In model (1) the change in the sign of $W_\theta$ is absorbed in the change of the anchoring axis of the surface from the normal to the tangential direction. Model (2) is similar to the observation of Porte [16] and corresponds to a planar-polar uniform axial structural transition at $\theta_0=61°$, where the free energy of the planar-polar structure $W_\theta R[1-2\sin(2\theta_0)/\pi]/2$ equals that of the uniform axial structure $\pi W_\theta R\cos^2\theta_0$ in the weak anchoring limit.

To resolve the question of whether the anchoring transition is of a discontinuous type [model (1)] or a continuous type [model (2)], we resort to optical observations of planar samples to eliminate the elastic constraint imposed by our curved geometries. The nematic liquid crystal 5CB was sandwiched between two alumina substrates treated with an aliphatic acid surfactant of different carbon number. The cell spacing was controlled to 20 $\mu$m with glass spacers. The alumina substrates were oriented such that their birefringence effects were compensated. Using conoscopy we confirmed the actual alignment at planar substrates to help us choose the correct model to describe our structural and anchoring transition. The $n>7$ surfaces are showing a black Maltese cross characteristic of homeotropic anchoring and a symmetric hyperbolic pattern for $n=5$ and 6 surfaces, indicative of planar alignment for the 2% samples. The same experiment was performed on the 4% sample to confirm the anchoring direction. This indicates that our anchoring transition is of a discontinuous type, informing us that $W_\theta$ decreases as $n$ decreases in supporting homeotropic anchoring until $W_\theta$ changes sign, forcing the anchoring to become planar.

The structural transition thus occurs at $W_\theta=0$, where the free energies of the planar-polar and parallel axial structures are equal. According to theory this indicates the dominance of short range interactions [63] rather than quadrupole ones [76]. Our results indicate that the 4% aliphatic acid sample exhibits the weakest anchoring energies of all the samples we studied since it goes through the $W_\theta=0$ point on aproaching the nematic-isotropic transition.

Information on the relationship between $W_\theta$ and the orientational order parameters can also be obtained. The planar-polar director-field is sensitive to the dimensionless surface parameter $RW_\theta/K$ and can only revert to the parallel axial structure if $W_\theta/K$ weakens. It is well

known that $K \sim S^2$ [75], but the relationship between $W_\theta$ and $S$ is not completely understood. If we assume that $W_\theta$ roughly obeys the power law $W_\theta \sim S^\beta$, our observed anchoring transition for the 4% $n=6$ sample indicates that $\beta > 2$, so the ratio $RW_\theta/K$ weakens as the nematic-isotropic transition is approached. If $\beta < 2$, the ratio $W_\theta/K$ would strengthen as the nematic-isotropic transition is approached, which is not the csae. Our observation that $\beta > 2$ is consistent with measurements of Erdmann and co-workers in PDLC droplets [77]. To obtain a better quantitative understanding of this liquid-crystal–surfactant interface, we resort to the study of pretransitional surface-induced order above the nematic-isotropic transition temperature.

## V. ISOTROPIC PHASE

### A. Landau–de Gennes formalism

We employ the Landau–de Gennes approach for the nematic-isotropic transition that is used to give a phenomenological expression for the free energy density close to the nematic-isotropic transition temperature. We follow our preliminary investigation [31], which showed that in both homeotropic and planar alignment of the liquid crystals the surface-induced ordering is uniaxial. Therefore for such systems with a uniform director orientation, the free energy density can be expanded in terms of a single scalar orientational order parameter $S$:

$$f(S)=f_0+\tfrac{1}{2}a(T-T^*)S^2-\tfrac{1}{3}bS^3+\tfrac{1}{4}cS^4+\tfrac{1}{2}L\left[\frac{dS}{dr}\right]^2 +\tfrac{1}{2}g(S-S_S)^2\delta(z)\ , \tag{7}$$

where $f_0$ is the order parameter independent part of the free energy density; $r$ is the distance from the cavity wall; and $a$, $b$, $c$, $L$, and $T^*$ are material parameters. The material parameters reported for 5CB are $a=0.13\times10^6$ J/m$^3$ K, $b=1.6\times10^6$ J/m$^3$, $c=3.9\times10^6$ J/m$^3$, $L=1.7\times10^6$ J/m, and $T_{NI}-T^*=2b^2/9ac=1.1$ K [78]. The final term in Eq. (4) is the surface free energy contribution first proposed by Durand [64], where $g$ is the coupling constant and $S_S$ is the preferred degree of order at the surface that strongly depends on the surface. This is similar to the two-parameter model employed by Sluckin and Poniewierski [32] of the form $(-GS+\frac{1}{2}US^2)\delta(z)$, where $G$ and $U$ are constants characterizing ordering and disordering of the surface, respectively. For comparison, $G$ and $U$ are related to $g$ and $S_S$ by the relations $G=2gS_S$, $U=2g$, and $S_S=G/U$. The effects of curvature introduced by our cylindrical tubes are neglected because studies of $T_{NI}$ shifts in droplets of comparable radii are $<0.1$ K [54]. This small shift is due to the curvature constraint being a factor $(\xi/R)^2 \ll 1$ smaller than the $f(S)$ term including $dS/dr$.

To derive the adsorption parameter $\Gamma_{LdG}$ within the Landau–de Gennes formalism, a contact nature for the surface interactions is assumed:

$$\Gamma_{LdG}=\int_0^\infty S(z)dz = 4\xi\sqrt{a(T-T^*)/2c}\,\ln\left[\frac{\sqrt{2/a(T-T^*)c}\,(\Lambda+b/3)+1}{\sqrt{2/a(T-T^*)c}\,(\Lambda+b/3)-1}\right]$$

with

$$\Lambda(S_0)=S_0^{-1}[2a(T-T^*)]^{1/2}[a(T-T^*)/2-bS_0/3+cS_0^2/4]^{1/2}+a(T-T^*)/S_0-b/3\ , \tag{8}$$

where $\xi=\xi_0(T/T^*-1)^{-\alpha}$ is the correlation length, $\alpha=\frac{1}{2}$ and $\xi_0$ being the standard temperature correlation length defined by $\xi_0=L/(aT^*)$ with $\xi_0=0.65$ nm for 5CB. $\Gamma_{LdG}$ exhibits a logarithmic singularity $\ln[T/(T-T_{NI})]$ on approaching $T_{NI}$ if $S_0 > 2b/3c$, which is 0.27 for 5CB.

### B. Aliphatic acid surfactant

Spectra recorded above the isotropic-nematic transition temperature for various surfaces of the 2% aliphatic acid surface treatment are presented in Fig. 7(a), showing an interesting development of the quadrupole splitting as $n$ is varied. For $n=7$, 9, and 15 surfaces, which induce homeotropic anchoring, $\langle\delta\nu\rangle$ increases as $n$ increases. The unresolvable peak, at $n=7$ also indicates the presence of very weak interfacial coupling. The splitting is again resolvable for $n=6$, where the anchoring is planar. The temperature dependence for the $n=15$, 9, and 5 samples is presented in Fig. 7(b). Both $\xi$ and $S_0$ increase as the nematic-isotropic transition temperature is approached, resulting in $\langle\delta\nu\rangle$ increasing.

Figures 8(a) and 8(b) show the temperature dependence of $\langle\delta\nu\rangle$ for $n=15$, 9, 7, 6, and 5 samples (2% surface treatment solution) on linear and logarithmic temperature scales, respectively. Within our experimental error, it appears that the $n=15$ and 9 samples lead to a weak logarithmic divergence corresponding to complete wetting, as evident from Fig. 8(b). In the $n=5$ and 6 surface, however, $\Gamma$ definitely remains finite and weakly temperature dependent, corresponding to partial wetting. No splitting was observed for $n=7$, implying that $\langle\delta\nu\rangle$ is smaller than the linewidth ($<200$ Hz), implying further that $\Gamma<0.2$ nm, indicating weak partial wetting or no wetting at all.

Figures 9(a) and 9(b) show the results of $\langle\delta\nu\rangle$ on linear and logarithmic temperature scales for the $n=20$, 18, and 17 surfaces (2% surface treatment solution), where anchoring is also homeotropic. An interesting

phenomenon is observed. The $n=17$ surface yields the largest quadrupole splitting of any sample, indicating an optimal ordering surface. As $n$ increases, $\langle \delta\nu \rangle$ decreases, which is the opposite trend observed in the $n=7$, 9, and 15 samples. Figure 8(b) indicates that $n=17$ and 18 lead to a weak logarithmic divergence, while $\Gamma$ for the $n=10$ surface definitely remains finite, indicating partial wetting.

The temperature development of $\langle \delta\nu \rangle$ for the 4% aliphatic acid surface treatment solution is presented in Figs. 10(a) and 10(b) for $n=5$ and 15 on linear and logarithmic temperature scales, respectively. The $n=15$ sample appears to have a weak logarithmic divergence, as observed in Fig. 10(b), contrary to the $n=5$ surface, which indicates only partial wetting. The characteristics of the $n=6$ surface were not analyzed because both planar and homeotropic anchoring conditions coexist very close to the nematic-isotropic transition temperature as observed in the experiments in the nematic phase (Fig. 5). The anchoring direction was therefore uncertain.

### C. Benzoic acid

The temperature dependence of $\langle \delta\nu \rangle$ for a 2% benzoic surface treatment solution ($n=10$) is presented in Figs. 11(a) and 11(b) on linear and logarithmic temperature scales. It appears from Fig. 11(b) that this sample exhibits a weak logarithmic divergence.

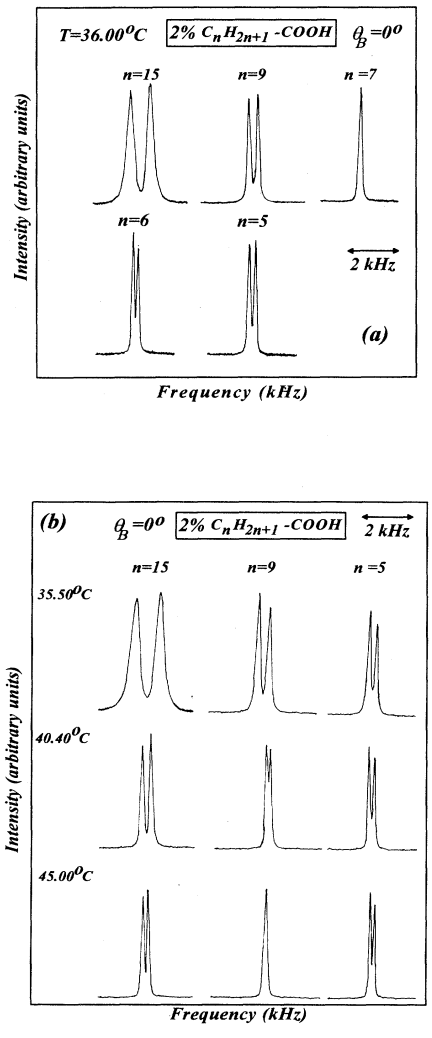


FIG. 7. $^2$H-NMR line shapes of 5CB-$\alpha d_2$ confined to the surfactant treated (2% $C_nH_{2n+1}$-COOH) cavities of Anopore membranes accumulated in the isotropic phase as a function of chain length of the aliphatic acid (a) at the surface and (b) as a function of temperature for several samples.

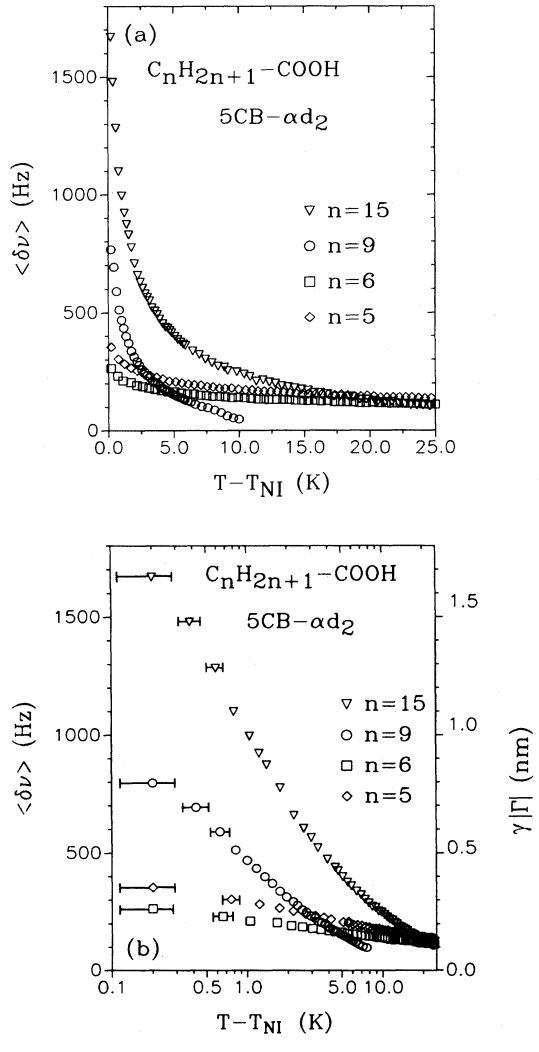


FIG. 8. The averaged quadrupole splitting frequency $\langle \delta\nu \rangle$ as a function of temperature on (a) a linear and (b) a semilog scale for the 2% $C_nH_{2n+1}$-COOH surface treatment for $n<15$. The semilog representation has the adsorption parameter $\Gamma$ plotted on the right $y$ axis, where $\gamma=1$ for $n=5$ and 6 and $\gamma=2$ for 9 and 15.

### D. Analysis of results in the isotropic phase

The orientational order parameter is derived at the cavity wall using the Landau–de Gennes approach supplemented by the surface layer correction (see Sec. III). The experimentally measured values of $\langle \delta\nu \rangle$ are derived by comparing $\Gamma$ to $\Gamma_{\mathrm{LdG}} + l_0 S_0$ and using Eqs. (8) and (4), yielding the temperature dependence of $S_0$. Since $^2$H-NMR cannot distinguish between negative and positive solutions of $S_0$, we simply choose $S_0 > 0$ for homeotropic anchoring conditions. For planar anchoring conditions, we choose the $S_0 < 0$ simply because our data show no evidence of a symmetry breaking transition on approaching the nematic-isotropic transition temperature.

To decipher whether the data really correspond to complete or partial wetting, the results are analyzed using a surface free energy density of the form $\frac{1}{2}g(S_0 - S_S)^2$ [64]. This form covers positive and negative ordering and the absence of a symmetry breaking transition. The surface coupling parameter $g$ and the preferred degree of ordering $S_S$ are determined such that the theoretical $S_0(T)$ dependence corresponds to the minimum total free energy and yields the best fit to $S_0$ obtained from $\Gamma$. To better the theoretical fits to the experimental data, the parameter $T_{\mathrm{NI}} - T^*$ is varied; this parameter should be close to 1.1 K to be consistent with theoretical predictions.

The values of $S_0$ and the theoretical fit to $S_0 = S_0(T)$ are presented in Fig. 12 for the 2% aliphatic acid surface treatment ($n = 15$, 9, 6, and 5). The temperature depen-

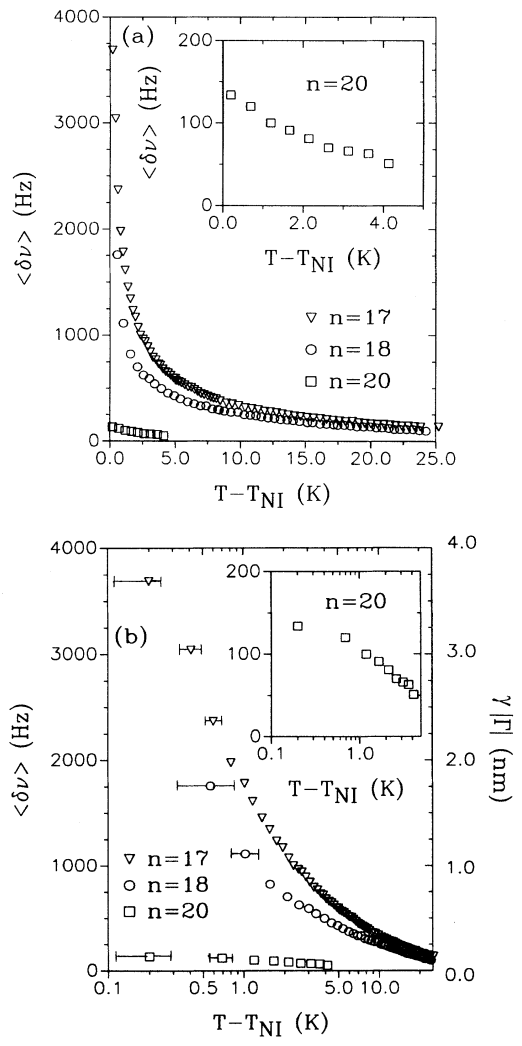


FIG. 9. The averaged quadrupole splitting frequency $\langle \delta\nu \rangle$ as a function of temperature on a (a) linear and (b) a semilog scale for the 2% $C_nH_{2n+1}$-COOH surface treatment for $n > 17$. The semilog representation has the adsorption parameter $\Gamma$ plotted on the right $y$ axis, where $\gamma = 1$ for all samples.

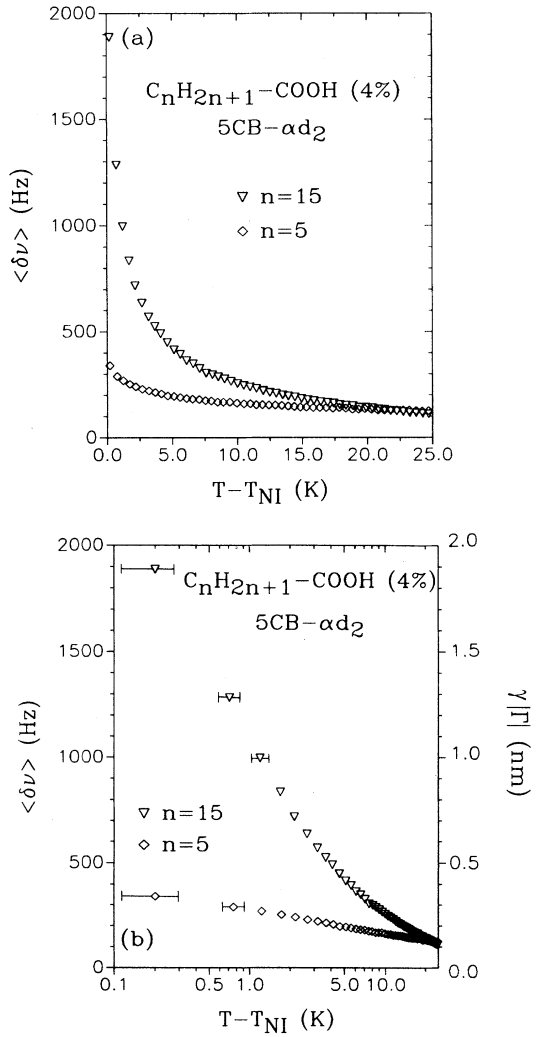


FIG. 10. The averaged quadrupole splitting frequency $\langle \delta\nu \rangle$ as a function of temperature on a (a) linear and (b) a semilog scale for the 4% $C_nH_{2n+1}$-COOH surface treatment for two different $n$. The semilog representation has the adsorption parameter $\Gamma$ plotted on the right $y$ axis, where $\gamma = 1$ for $n = 15$ and $\gamma = 2$ for $n = 5$.

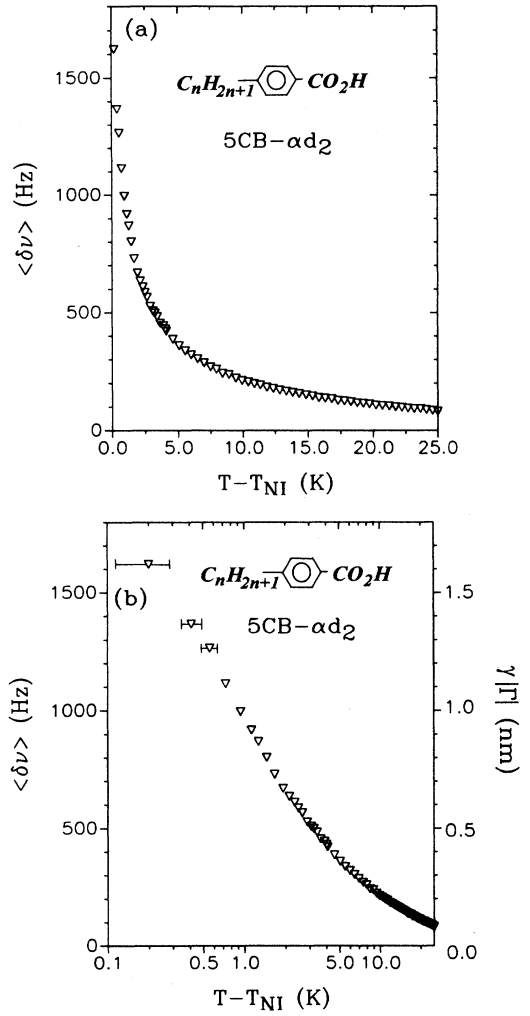


FIG. 11. The averaged quadrupole splitting frequency $\langle \delta\nu \rangle$ as a function of temperature on (a) a linear and (b) a semilog scale for the 2% benzoic acid surface treatment for $n=10$. The semilog representation has the adsorption parameter $\Gamma$ plotted on the right $y$ axis, where $\gamma=1$.

dence of $S_0$ shows a strong critical increase for $n=9$ and 15 and a noncritical behavior for $n=5$ and 6. In the fitting procedure for $n=5$ and 6 surfaces, the exponent on the correlation length is determined to be $\alpha=0.4\pm0.02$ instead of the classical 0.5 to compensate for the small but nonphysical increase of $S_0$ as the temperature increases. It is interesting to note that the magnitude of $S_0$ is slightly larger for $n=5$ than $n=6$ when planar anchoring results. This indicates that for these short chain surfactants, strong interactions between the alumina substrate and the core of the liquid-crystal molecules dominate the steric hindrance to enforce planar anchoring. The $n=15$ and 9 samples show a sharp increase in $S_0$ as the nematic-isotropic transition is approached, but within the experimental error of the NMR spectrometer ($T-T_{NI}>0.2$ K) the values of $S_0$ are still much smaller than the threshold value of $S_0>0.27$ needed for

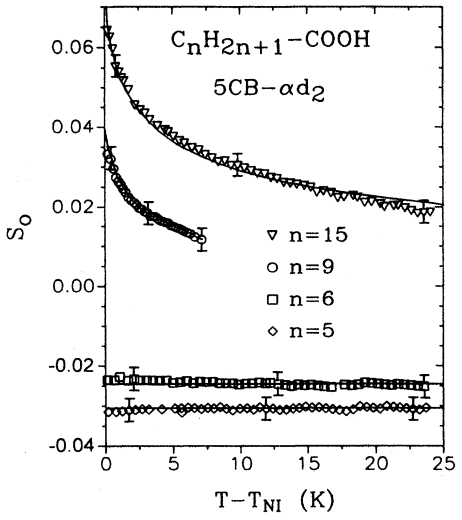


FIG. 12. The surface induced orientational order parameter $S_0$ versus reduced temperature for various lengths ($n$) of the surfactant molecule (2% $C_nH_{2n+1}$-COOH). The solid line denotes the theoretical fit.

the divergence of $\Gamma$ within the Landau–de Gennes model; therefore wetting cannot be completed. Nevertheless, the strong precritical increase of the adsorption parameter resembles the complete wetting situation rather than the partial wetting of $n=5$ and 6 cases; therefore we have decided to introduce the term *quasicomplete wetting* for the description of this behavior [31]. The fitting parameters are summarized in Table I.

It is interesting to compare our data on planar anchor-

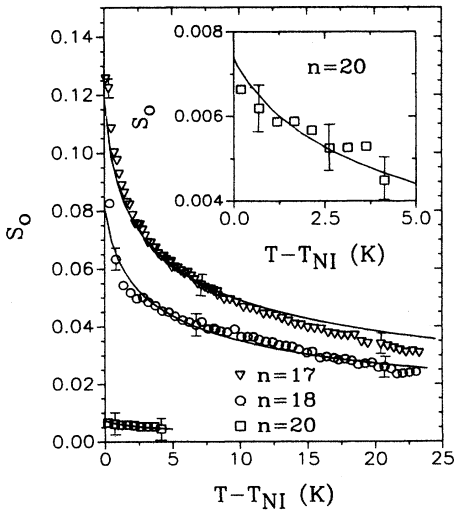


FIG. 13. The surface induced orientational order parameter $S_0$ versus reduced temperature for various lengths ($n$) of the surfactant molecule (2% $C_nH_{2n+1}$-COOH). The solid line denotes the theoretical fit.

ing ($n=5$ and 6 surfaces) to that of Moses and Shen [29]. For planar anchoring between planar, parallel substrates, they report values of $G=-6.8\times10^{-5}$ J/m$^2$, $U=9.0\times10^{-5}$ J/m$^2$, and $S_0=-0.0047$ near the nematic-isotropic transition temperature using the surface free energy of the form $f_S=-GS_0+\frac{1}{2}US_0^2$. Their values of $S_0$ and $G$ compare well with our $n=5$ and 6 samples, which exhibit similar degenerate planar anchoring; however, $U$ does not because their sample exhibits a stronger temperature dependence for $\Gamma$. Our large value of $U$ is related to the noncritical behavior of $S_0$ in our systems.

The values of $S_0$ for the long chain aliphatic acid surface treatments ($n=20$, 18, and 17) prepared with a 2% surface treatment solution are presented in Fig. 13. The optimal ordering surface in these systems is clearly the $n=17$ sample, which reaches order parameters at the surface near the nematic-isotropic transition that are slightly less than the bulk nematic just below the transition point. For larger $n$, the value of $S_0$ decreases; the $n=20$ sample exhibits very weak surface ordering, which is consistent with its partial wetting behavior. The surface order parameters for the $n=18$ and 17 samples are below the threshold value of $S_0>0.27$ for complete wetting in the Landau–de Gennes model; therefore wetting is only quasicomplete. The fitted values of $g$ and $S_S$ are presented in Table I.

The fitting parameters for the 2% aliphatic acid surfaces are plotted as a function of $n$ in Fig. 14. Figure 14(a) clearly shows that the optimal ordering surfaces is obtained for the $n=17$ sample, and it shows the regions that correspond to partial and quasicomplete wetting. The ordering capabilities of the surfactants rapidly fall off after $n=18$ and reenter the partial wetting regime. Figure 14(b) shows the empirical relationship between $g$ and $n$. The maximum value of $g$ for the homeotropically anchored systems occurs at $n=17$ since this is the optimal ordering surface. The large value of $g$ for the $n=5$ and 6 surfaces is required to obtain the noncritical temperature behaviors.

Our long aliphatic chains are of a length similar to the chains on the commonly used silane surfactant, which also promotes homeotropic anchoring: dimethyloctadecyl-3-(trimethoxysilyl) propylammonium chloride (DMOAP). Chen and co-workers [30] have measured the surface order parameter of 5CB on DMOAP covered surfaces at $S_0\sim0.2$ near the nematic-isotropic transition temperature. This is slightly larger than our $n=17$ surface, which reaches $S_0\sim0.13$ just above the nematic-isotropic transition temperature.

This suggests that the ordering mechanisms, which are predominantly sterical, are similar for both systems.

The temperature dependence of $S_0$ for the 4% aliphatic acid sample is presented in Fig. 15 and the fitting pa-

TABLE I. Estimated interfacial parameters for the coupling of 5CB molecules to surfactant covered ($C_nH_{2n+1}$-COOH) alumina surfaces.

| $n$ anchoring | Concentration | $T_{NI}-T^*$ (K) | $10^{-4}$ g (J/m$^2$) | $S_S$ | $10^{-4}$ G (J/m$^2$) | $10^{-3}$ U (J/m$^2$) | Wetting regime |
|---|---|---|---|---|---|---|---|
| 5 parallel[a] | 2% | 1.5±0.2 | >58.3 | −0.031±0.005 | >−3.61 | >11.1 | partial |
| 5 parallel[a] | 4% | 1.5±0.2 | >58.3 | −0.026±0.005 | >−3.02 | >11.1 | partial |
| 6 parallel[a] | 2% | 1.5±0.2 | >58.3 | −0.024±0.005 | >−.278 | >11.1 | partial |
| 6 parallel[a] | 4% | | | | | | |
| 7 homeotropic[b] | 2% | 1.1±0.3 | 7.30±1.50 | 0.008±0.02 | 0.12±0.05 | 1.46±3.00 | partial |
| 9 homeotropic | 2% | 0.8±0.3 | 7.80±1.00 | 0.05±0.01 | 0.78±0.25 | 1.56±1.50 | quasicomplete |
| 15 homeotropic | 2% | 1.1±0.2 | 8.75±1.00 | 0.11±0.02 | 1.92±0.60 | 1.75±2.00 | quasicomplete |
| 15 homeotropic | 4% | 1.1±0.2 | 9.20±1.0 | 0.12±0.02 | 2.21±0.60 | 1.84±2.00 | quasicomplete |
| benzoic homeotropic | 2% | 1.1±0.2 | 9.04±1.00 | 0.11±0.02 | 1.98±0.60 | 1.81±2.00 | quasicomplete |
| 17 homeotropic | 2% | 1.1±0.2 | 9.91±1.00 | 0.18±0.02 | 3.37±0.70 | 1.98±2.00 | quasicomplete |
| 18 homeotropic | 2% | 1.1±0.2 | 9.04±1.00 | 0.13±0.02 | 2.35±0.70 | 1.81±2.0 | quasicomplete |
| 20 homeotropic | 2% | 1.1±0.3 | 8.45±1.50 | 0.014±0.005 | 0.24±0.10 | 1.70±3.00 | partial |

[a]Only lower bound on $g$, $G$, and $U$ attainable.
[b]Estimate based on linewidth measurements.

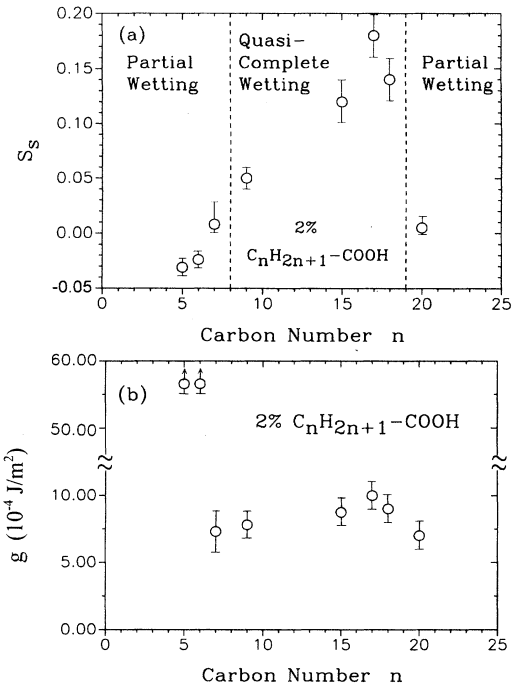


FIG. 14. (a) The preferred degree of order $S_S$ and (b) the surface coupling strength $g$ as a function of chain length $n$ of the $C_nH_{2n+1}$-COOH surfactant for the 2% sample.

rameters are summarized in Table I. Comparing the 2% and 4% samples for the $n=15$ sample, we see that the value of $S_S$ is slightly larger for the 4% surface treatment than for the 2% one. This indicates that in the case where steric hindrance induces homeotropic anchoring,

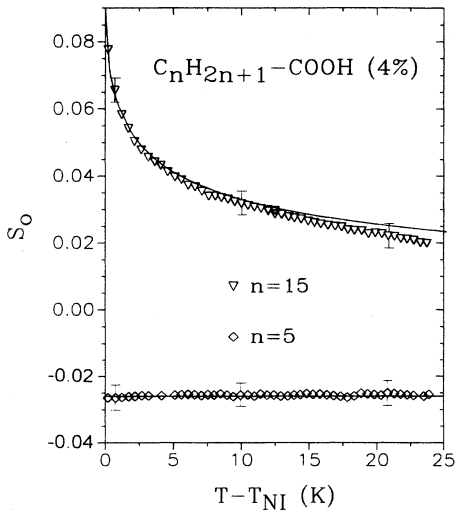


FIG. 15. The surface induced orientational order parameter $S_0$ versus reduced temperature for various lengths ($n$) of the surfactant molecule (4% $C_nH_{2n+1}$-COOH). The solid line denotes the theoretical fit.

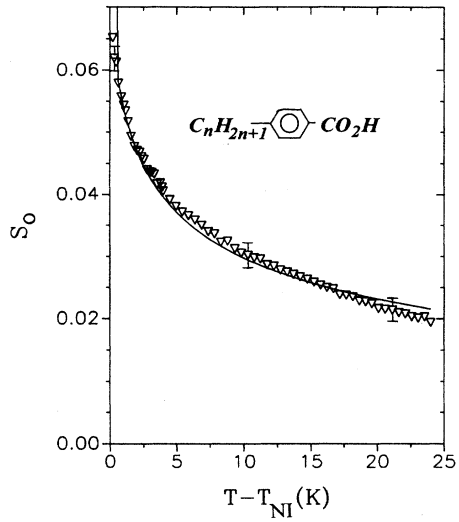


FIG. 16. The surface induced orientational order parameter $S_0$ versus reduced temperature for various lengths $n=10$ of the benzoic acid surfactant molecule (2%). The solid line denotes the theoretical fit.

the higher concentration of the surfactant molecules has only a nominal effect on the surface order. Comparison of the 2% and 4% samples for $n=5$ shows that $S_s$ is slightly smaller in magnitude for the 4% sample than for the 2% one. This is consistent with our earlier statement concerning the interaction of the core of the liquid-crystal molecules with the alumina surface underneath the surfactant monolayer because the higher concentration of surfactant molecules in the 4% sample keeps the core away from the surface. The larger concentration of surfactant molecules on the surface appears to weaken the liquid core-alumina interaction.

The analysis of the 2% benzoic acid surfactant is presented in Fig. 16. The benzoic molecule was chosen to investigate how a rigid core on the surfactant molecule influences the ordering of the liquid-crystal molecules. The theoretical fits to the data indicate that $g$ and $S_S$ are similar to those for the 2% aliphatic acid surface treatment with $n=15$ (see Table I). This indicates that the rigid core of the benzoic acid has less influence on the ordering of the liquid-crystal molecules than a more flexible aliphatic chain. A possible explanation for these similarities may be that the interdigitation of the liquid-crystal molecules in the surfactant monolayer is minimal, and the more rigid aromatic core has little influence on the ordering of the liquid-crystal molecules.

## VI. CONCLUSIONS

A comprehensive study on anchoring and wetting and ordering near the nematic-isotropic transition temperature is presented. In the nematic phase the observation of a discontinuous homeotropic-to-planar anchoring transition indicates that interfacial coupling is dominated

by short range interactions rather than quadrupolar ones [21]. The transition occurring between $n=6$ and 7 (for 2% surface treatment) shifts to smaller carbon number $n$ (between $n=5$ and 6) as the density of the surfactant molecules at the surface increases (4% surface treatment solution). The discontinuous anchoring transition is also seen as a function of temperature on approaching the nematic-isotropic transition from below, indicating that the relationship between $W_\theta$ and $S$ is $W_\theta \sim S^\beta$ with $\beta > 2$, which is consistent with the findings of Erdmann, Žumer, and Doane [77].

The studies of the pretransitional ordering on approaching the nematic-isotropic transition temperature from above unveil a variety of wetting phenomena, indicating a strong dependence of the interfacial coupling strength on the nature of the surfactant monolayer. In addition to the anchoring transition from the planar-to-homeotropic ordering, our observations show two wetting transitions in the homeotropic regime as the length of our surfactant molecule on the surface is varied from $n=7$ to 20 [see Fig. 14(a)]. An orientational wetting transition from partial to quasicomplete between $n=7$ and 9 and another wetting transition from quasicomplete to partial wetting between $n=18$ and 20 are observed. We attribute the first wetting transition from partial to quasicomplete as an increase in the steric interactions with increasing chain length. The reentrant wetting transition from quasicomplete to partial indicates that with increasing surfactant chain length, the surfactant tail in the aligning surface layer undergoes a type of "melting" transition. The lack of the complete wetting in this case seems to be a result of relatively weak short range interactions [63] rather than confinement [76]. The optimal ordering surface occurs at $n=17$ for the 2% aliphatic acid surface treatment. Unfortunately, the coupling strength is still not strong enough for the Sheng-type prewetting boundary layer transition [4]. The density of surfactant molecules in the ordering monolayer has only a small influence on the orientational order parameter at the surface. The value of $S_0$ is enhanced by $\sim 10\%$ for $n=15$ when the surface treatment solution is changed from 2% to 4%.

In the planar anchoring situation corresponding to surfactants with $n=5$ and 6, the weak temperature dependence of the surface order and its persistence deep into the isotropic phase indicate the need for inclusion of nonlinear terms in the phenomenological treatment of surface coupling. The lack of the symmetry breaking BKT transition in these cases indicates that interfacial coupling is not strong enough to induce such a transition. A search for a method to enhance the surface coupling in planar anchored systems is in progress. Investigations on the order parameter of the surfactant monolayer is planned, and we are continually searching for surface treatments that give rise to strong interfacial coupling.

## ACKNOWLEDGMENTS

Research was supported by the National Science Foundation Solid State Chemistry Grant Nos. DMR 91-20130 and ALCOM DMR 89-20147. S.Ž. acknowledges the support of the Ministry of Science and Technology of Slovenia (Grant No. J1 5034-790-95) and by ALCOM during his visits to the Liquid Crystal Institute. The 5CB-$\alpha d_2$ was synthesized by Sandra Keast and Mary Neubert and is greatly appreciated.

[1] A. Poniewierski and T. J. Sluckin, in *Fluids Interfacial Phenomena,* edited by C. Croxton (Wiley, New York, 1986), Chap. 5, and references therein.
[2] D. W. Allender, G. L. Henderson, and D. L. Johnson, Phys. Rev. A **24**, 1086 (1981).
[3] A. Mauger, G. Zribi, D. L. Mills, and J. Toner, Phys. Rev. Lett. **53**, 2485 (1984).
[4] P. Sheng, Phys. Rev. Lett. **37**, 1059 (1976); Phys. Rev. A **26**, 1610 (1982).
[5] B. Jerome, Rep. Prog. Phys. **54**, 391 (1991).
[6] K. Miyano, Phys. Rev. Lett. **43**, 51 (1979); J. Chem. Phys. **71**, 4108 (1979); J. Tarczon and K. Miyano, *ibid.* **73**, 1994 (1980).
[7] G. Ryschenkow and M. Kleman, J. Chem. Phys. **64**, 404 (1976).
[8] K. Hiltrtrop and H. Stegemeyer, Liq. Cryst. Ordered Fluids **4**, 515 (1983).
[9] H. Bireki, Liq. Cryst. Ordered Fluids **4**, 853 (1983).
[10] G. E. Volovik and O. D. Lavrentovich, Zh. Eksp. Teor. Fiz. **85**, 1997 (1983) [Sov. Phys. JETP **58**, 1159 (1983)].
[11] G. A. Di Lisi, C. Rosenblat, A. C. Griffin, and U. Hari, Liq. Cryst. **7**, 353 (1990).
[12] K. Flatischler, L. Komitov, S. T. Lagerwall, B. Stebler, and A. Strigazzi, Mol. Cryst. Liq. Cryst. **198**, 119 (1991).
[13] L. Komitov, B. Stebler, G. Gabrielli, M. Puggelli, A. Sparavigna, and A. Strigazzi, Mol. Cryst. Liq. Cryst. **243**, 107 (1994).
[14] J. S. Patel and H. Yokoyama, Nature (London) **362**, 525 (1993).
[15] J. Bechhoefer, J.-L. Duvail, L. Masson, B. Jerome, R. M. Hornreich, and P. Pieranski, Phys. Rev. Lett. **64**, 1911 (1990).
[16] G. Porte, J. Phys. (Paris) **10**, 1245 (1976).
[17] P. Pieranski and B. Jerome, Phys. Rev. A **43**, 317 (1989); Mol. Cryst. Liq. Cryst. **199**, 167 (1991).
[18] H. S. Kitzerow, B. Jerome, and P. Pieranski, Physica A **174**, 163 (1991).
[19] K. Hiltrop and H. Stegemeyer, Bunsenges Phys. Chem. **85**, 582 (1981).
[20] V. G. Nazarenko and O. D. Lavrentovich, Phys. Rev. E **49**, R990 (1994).
[21] P. I. C. Teixeira and T. J. Sluckin, J. Chem. Phys. **97**, 1498 (1992).
[22] B. M. Ocko, A. Braslau, P. S. Pershan, J. Als-Nielsen, and M. Deutsch, Phys. Rev. Lett. **57**, 94 (1986).
[23] B. M. Ocko, Phys. Rev. Lett. **64**, 2160 (1990).

[24] T. Stoebe, R. Geer, C. C. Huang, and J. W. Goodby, Phys. Rev. Lett. **69**, 2090 (1992).
[25] Z. Pawlowska, G. F. Kventsel, and T. J. Sluckin, Phys. Rev. A **36**, 992 (1987); **38**, 5342 (1988).
[26] J. V. Selinger and D. R. Nelson, Phys. Rev. A **37**, 1736 (1988).
[27] G. Barberi and G. Durand, Phys. Rev. A **41**, 2207 (1990).
[28] G. Barberi and G. Durand, J. Phys. (France) II **1**, 651 (1991).
[29] T. Moses and Y. R. Shen, Phys. Rev. Lett. **67**, 2033 (1991).
[30] W. Chen, L. J. Martinez-Miranda, H. Hsiung, and Y. R. Shen, Phys. Rev. Lett. **62**, 1860 (1989); Mol. Cryst. Liq. Cryst. **179**, 419 (1990).
[31] G. P. Crawford, R. Ondris-Crawford, S. Žumer, and J. W. Doane, Phys. Rev. Lett. **70**, 1838 (1993); Liq. Cryst. **14**, 1573 (1993).
[32] T. J. Sluckin and A. Poniewierski, Phys. Rev. Lett. **55**, 2907 (1985).
[33] R. M. Hornreich, E. I. Kats, and V. V. Lebedev, Phys. Rev. A **46**, 4935 (1992).
[34] Y. L'vov, R. M. Hornreich, and D. W. Allender, Phys. Rev. E **48**, 1115 (1993); N. Kothekar, D. W. Allender, and R. M. Hornreich, *ibid.* **49**, 2150 (1994).
[35] P. Sheng, B.-Z. Li, M. Zhou, T. Moses, and Y. R. Shen, Phys. Rev. A **46**, 946 (1992).
[36] B. Jerome, J. O'Brien, Y. Ouchi, C. Stanners, and Y. R. Shen, Phys. Rev. Lett. **71**, 758 (1993).
[37] J. Dolinšek, O. Jarh, M. Vilfan, S. Žumer, R. Blinc, J. W. Doane, and G. P. Crawford, J. Chem. Phys. **95**, 2154 (1991).
[38] G. P. Crawford, R. Stannarius, and J. W. Doane, Phys. Rev. A **44**, 2558 (1991).
[39] G. P. Crawford, D. K. Yang, S. Žumer, D. Finotello, and J. W. Doane, Phys. Rev. Lett. **66**, 723 (1991).
[40] D. W. Allender, G. P. Crawford, and J. W. Doane, Phys. Rev. Lett. **67**, 1442 (1991); Phys. Rev. A **45**, 8693 (1992).
[41] G. S. Iannacchione, G. P. Crawford, S. Žumer, J. W. Doane, and D. Finotello, Phys. Rev. Lett. **71**, 2595 (1993).
[42] R. Ondris-Crawford, G. P. Crawford, S. Žumer, and J. W. Doane, Phys. Rev. Lett. **70**, 197 (1993).
[43] N. Vrbančič, M. Vilfan, R. Blinc, J. Dolinšek, G. P. Crawford, and J. W. Doane, J. Chem. Phys. **98**, 3540 (1993).
[44] R. Ondris-Crawford, G. P. Crawford, S. Žumer, J. W. Doane, M. Vilfan, and I. Vilfan, Phys. Rev. E **48**, 1998 (1993).
[45] I. Vilfan, M. Vilfan, and S. Žumer, Phys. Rev. A **40**, 4724 (1989).
[46] G. S. Iannacchione and D. Finotello, Phys. Rev. Lett. **69**, 2094 (1992).
[47] F. M. Aliev and M. N. Breganov, Zh. Eksp. Teor. Fiz. **95**, 122 (1899) [Sov. Phys. JETP **68**, 70 (1989)].
[48] T. Bellini, N. A. Clark, C. D. Muzny, L. Wu, C. W. Garland, D. W. Schaefer, and B. J. Oliver, Phys. Rev. Lett. **69**, 788 (1992).
[49] S. Kralj, G. Lahajnar, A. Zidanšek, N. Vrbančič-Kopač, M. Vilfan, R. Blinc, and M. Kosec, Phys. Rev. E **48**, 340 (1993).
[50] X. Wu, W. I. Goldburg, M. X. Liu, and J. Z. Xue, Phys. Rev. Lett. **69**, 470 (1992).
[51] S. Kralj and S. Žumer, Phys. Rev. A **45**, 2461 (1992); Liq. Cryst. **12**, 613 (1992).
[52] C. Chiccoli, P. Pasini, F. Semeria, and C. Zannoni, Phys. Lett. A **150**, 311 (1990); Mol. Cryst. Liq. Cryst. **212**, 197 (1992); **221**, 19 (1992).
[53] E. Berggren, C. Zannoni, C. Chiccoli, P. Pasini, and F. Semeria, Chem. Phys. Lett. **197**, 224 (1992); Phys. Rev. E **49**, 614 (1994).
[54] S. Kralj, S. Žumer, and D. W. Allender, Phys. Rev. A **43**, 2943 (1991).
[55] I. Vilfan, M. Vilfan, and S. Žumer, Phys. Rev. A **40**, 4724 (1989).
[56] J. Cognard, Mol. Cryst. Liq. Cryst. Suppl. **1**, 1 (1982).
[57] J. W. Doane, in *Liquid Crystals: Applications and Uses,* edited by B. Bahadur (World Scientific, Singapore, 1990), Chap. 14.
[58] A. Rapini and M. Papoular, J. Phys. (Paris) Colloq. **30**, C4-45 (1969).
[59] D. Riviere, Y. Levy, and E. Guyon, J. Phys. (Paris) Lett. **40**, L215 (1979).
[60] H. Yokoyama and H. A. van Sprang, J. Appl. Phys. **57**, 4520 (1985).
[61] A. Golemme, S. Žumer, D. W. Allender, and J. W. Doane, Phys. Rev. Lett. **61**, 1937 (1988).
[62] A. Golemme, S. Žumer, J. W. Doane, and M. E. Neubert, Phys. Rev. A **37**, 559 (1988).
[63] T. J. Sluckin and A. Poniewierski, Mol. Cryst. Liq. Cryst. **179**, 349 (1979).
[64] M. Nobili and G. Durand, Phys. Rev. A **46**, R6174 (1992).
[65] G. P. Crawford, L. M. Steele, R. Ondris-Crawford, G. S. Iannacchione, C. J. Yeager, J. W. Doane, and D. Finotello, J. Chem. Phys. **96**, 788 (1992).
[66] R. C. Furneaus, W. R. Rigby, and A. P. Davidson, Nature (London) **337**, 147 (1989).
[67] J. Hoffman, Astron. Lab. **21**, 70 (1989).
[68] G. S. Iannacchione and D. Finotello, Phys. Rev. **50**, 4780 (1994).
[69] J. W. Doane, in *Magnetic Resonance of Phase Transitions,* edited by F. J. Owens, C. P. Poole, and H. A. Farach (Academic, New York, 1979), Chap. 4.
[70] G. P. Crawford, M. Vilfan, J. W. Doane, and I. Vilfan, Phys. Rev. A **43**, 835 (1991).
[71] P. E. Cladis and M. Kleman, J. Phys. (Paris) **33**, 591 (1972).
[72] R. B. Meyer, Philos. Mag. **27**, 405 (1973).
[73] A. Saupe, Mol. Cryst. Liq. Cryst. **21**, 211 (1973).
[74] S. Kralj and S. Žumer, Liq. Cryst. **15**, 521 (1993).
[75] S. Kralj and S. Žumer, Phys. Rev. E **51**, 366 (1995).
[76] A. Poniewierski and T. J. Sluckin, Liq. Cryst. **2**, 281 (1987).
[77] J. H. Erdmann, S. Žumer, and J. W. Doane, Phys. Rev. Lett. **64**, 1907 (1990).
[78] H. J. Coles, Mol. Cryst. Liq. Cryst. **49**, 67 (1978).

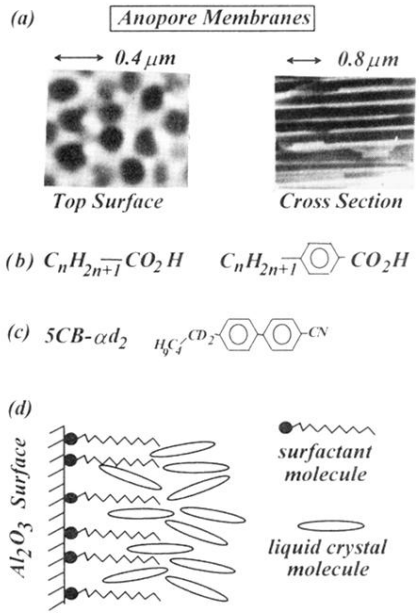


FIG. 1. Scanning electron microscope photograph of Anopore membranes (a) showing the cylindrical nature of the confining pores. (b) The aliphatic and benzoic acid surfactants used to treat the inner cavity wall of the $Al_2O_3$ Anopore membranes. (c) The deuterated low molecular weight liquid-crystal 5CB deuterated in the $\alpha$ position on the hydrocarbon chain. (d) A simple model to demonstrate the interaction between the aliphatic acid surface treatment and the liquid-crystal molecules.